View metadata, citation and similar papers at core.ac.uk

brought to you by CORE

provided by CORE

Wright State University

CORE Scholar

Physics Faculty Publications

Physics

2-1-2010

Structural Investigations and Magnetic Properties of Sol-Gel Ni0.5Zn0.5Fe2O4 Thin Films for Microwave Heating

Pengzhao Z. Gao

Evgeny V. Rebrov

Tiny M. W. G. M. Verhoeven

Jaap C. Schouten

Richard Kleismit

See next page for additional authors

Follow this and additional works at: https://corescholar.libraries.wright.edu/physics

 Part of the Physics Commons

Repository Citation

Gao, P. Z., Rebrov, E. V., Verhoeven, T. M., Schouten, J. C., Kleismit, R., Kozlowski, G., Cetnar, J. S., Turgut, Z., & Subramanyam, G. (2010). Structural Investigations and Magnetic Properties of Sol-Gel Ni0.5Zn0.5Fe2O4 Thin Films for Microwave Heating. *Journal of Applied Physics, 107* (4), 44317. https://corescholar.libraries.wright.edu/physics/165

This Article is brought to you for free and open access by the Physics at CORE Scholar. It has been accepted for inclusion in Physics Faculty Publications by an authorized administrator of CORE Scholar. For more information, please contact library-corescholar@wright.edu.

Authors

Pengzhao Z. Gao, Evgeny V. Rebrov, Tiny M. W. G. M. Verhoeven, Jaap C. Schouten, Richard Kleismit, Gregory Kozlowski, John S. Cetnar, Zafer Turgut, and Guru Subramanyam

This article is available at CORE Scholar: https://corescholar.libraries.wright.edu/physics/165

Structural investigations and magnetic properties of sol-gel $Ni_{0.5}Zn_{0.5}Fe_2O_4$ thin films for microwave heating

Pengzhao Gao,[1,a)] Evgeny V. Rebrov,[1,b),c)] Tiny M. W. G. M. Verhoeven,[1] Jaap C. Schouten,[1] Richard Kleismit,[2] Gregory Kozlowski,[2] John Cetnar,[2] Zafer Turgut,[3] and Guru Subramanyam[4]

[1]*Eindhoven University of Technology, P.O. Box 513, 5600 MB Eindhoven, The Netherlands*
[2]*Department of Physics, Wright State University, Dayton, Ohio 45435, USA*
[3]*Air Force Research Laboratory, Wright-Patterson AFB, Ohio 45433, USA*
[4]*Department of Electrical and Computer Engineering, University of Dayton, Dayton, Ohio 45469, USA*

(Received 2 September 2009; accepted 12 January 2010; published online 26 February 2010)

Nanocrystalline $Ni_{0.5}Zn_{0.5}Fe_2O_4$ thin films have been synthesized with various grain sizes by a sol-gel method on polycrystalline silicon substrates. The morphology, magnetic, and microwave absorption properties of the films calcined in the 673–1073 K range were studied with x-ray diffraction, scanning electron microscopy, x-ray photoelectron spectroscopy, atomic force microscopy, vibrating sample magnetometry, and evanescent microwave microscopy. All films were uniform without microcracks. Increasing the calcination temperature from 873 to 1073 K and time from 1 to 3 h resulted in an increase of the grain size from 12 to 27 nm. The saturation and remnant magnetization increased with increasing the grain size, while the coercivity demonstrated a maximum near a critical grain size of 21 nm due to the transition from monodomain to multidomain behavior. The complex permittivity of the Ni–Zn ferrite films was measured in the frequency range of 2–15 GHz. The heating behavior was studied in a multimode microwave cavity at 2.4 GHz. The highest microwave heating rate in the temperature range of 315–355 K was observed in the film close to the critical grain size. © *2010 American Institute of Physics*. [doi:10.1063/1.3309767]

I. INTRODUCTION

A. Concept of microwave heating with ferrite thin films

Microwave heating has become an important method for chemical reactor heating and materials processing. The concept of microwave heating enables optimal control of the rate of heat transfer in a microstructured reactor by eliminating conductive and/or convective heat transport resistances. In this way the controlled heating of a microreactor can be achieved using selective microwave absorption into a functional thin film (i.e., with thickness $<1.0\ \mu m$) deposited on the microchannel walls. Ni–Zn ultrafine spinel type ferrites are possible candidates for microwave heating due to their moderate dielectric losses in the range between 2 and 15 GHz as well as large magnetic losses.[1–3]

Spinel ferrites have the general molecular formula $M^{2+}Fe_2^{3+}O_4^{2-}$, where divalent metal cations M^{2+} and Fe^{3+} occupy tetrahedral (A) and octahedral (B) interstitial positions of the fcc lattice formed by O_2^{2-} ions. Both dielectric and magnetic properties of these oxides depend on the type of cations and their distribution among the two interstitial positions, which in turn depends on the method of synthesis and calcination conditions[4,5] and the film density.[6] The grain size increases with increasing calcination temperature of NiZn ferrites[7,8] and the dielectric constant increases when the grain grows.[9]

The cation distribution and the resulting magnetic properties are found to be different in some nanocrystalline spinel ferrites when compared to those of their bulk counterparts. In the bulk form $ZnFe_2O_4$ is a normal spinel with Zn^{2+} ions at the A sites and Fe^{3+} ions at the B sites, and it exhibits antiferromagnetic ordering below 10 K. Nanocrystalline $ZnFe_2O_4$ with a grain size of about 10–20 nm is magnetically ordered with a large magnetic moment even at high temperatures.[10,11] The observed high temperature magnetic ordering is attributed to the change in the cation distribution from the normal to the mixed spinel type where Fe^{3+} and Zn^{2+} ions occupy both sites.[12] $NiFe_2O_4$ has the mixed spinel structure when the grain size is reduced to a few nanometers.[4] It exhibits noncollinear spin structure and the magnetic moment is appreciably lower than the value for the bulk material.[13] A model wherein the particle consists of a core with the collinear spin arrangement and a surface layer with the magnetic moment inclined to the direction of magnetization has been proposed.[13]

Ferrite films are usually prepared by sputtering,[14] pulsed laser deposition,[15] and spray coating[16] processes. On the other hand, sol-gel[17–19] and hydrothermal[20] routes of ferrite synthesis have shown increasing importance. The advantages of the sol-gel process are high purity, chemical homogeneity, small and uniform particle size, and controlled grain shape. However, the Ni–Zn ferrite single phase can only be formed after calcination at temperatures above 1100 K. The formation of microcracks in ferrite films during calcination is con-

[a)]Present address: College of Materials Science and Engineering, Human University, 410082 Changsha, China.
[b)]On sabbatical leave at the Physics Department, Wright State University, Dayton, OH 45435, USA.
[c)]Author to whom correspondence should be addressed. Electronic mail: e.rebrov@tue.nl.

 © 2010 American Institute of Physics

sidered to be a disadvantage which limits application of the sol-gel method.[21] To obtain crack-free films, vacuum extraction was applied during heat treatment.[22] Preparation of ferrite/SiO_2 composite films with 5–30 wt % ferrite content[23] is another method to eliminate microcracks. However, the morphology of the resulting composite films is difficult to control. An addition of 1–3 wt % $5PbO \cdot SiO_2$ or $5PbO \cdot B_2O_3$ powders was found to be effective to obstruct the movement of grain boundaries and to minimize the ferrite grain size.[24] The addition of Zn in the ferrite composition has also been known to play a crucial role in lowering the firing temperature. However, there are no comprehensive studies on a structure—microwave heating relationship for the Ni–Zn ferrite films in the literature. For ferrite thin films having a thickness on a nanoscale, the grain size is also in the nanometer range scale, which is much smaller than the skin depth. Due to this unique feature, the heating behavior of ferrite thin films is different from the bulk ferrite materials.

B. Measurements of dielectric properties of thin films

Measurements of the dielectric properties of Ni–Zn ferrite films at microwave frequencies 2–15 GHz are performed by using a scanning evanescent microwave microscope as reported elsewhere.[25,26] In performing quantitative measurements of the electromagnetic properties, the detailed electrostatic field configuration outside the tip is required. The probe tip and film must be considered as a whole and the solution of the electrostatic field equations at appropriate boundary conditions has to be obtained. This relates the tip-film distance to the relative resonant frequency shift of the resonator $\Delta f/f$, the change in the reciprocal quality factor $\Delta(1/Q)$ and physical ferrite film properties for a given probe geometry. To calculate a local surface permittivity of films we are using our theoretical two-point model[27] which requires to measure only two extreme values of the frequency and quality factor: one pair, f_0 and Q_0, when the tip is well separated from the film (not interacting with the film) and another pair, f and Q, when the tip touches the film surface. Our model relates the changes $\Delta f/f$ and $\Delta(1/Q)$ between these two positions to the real and imaginary parts ε_1 and ε_2 of the dielectric constant $[\varepsilon=\varepsilon'-i\varepsilon''=\varepsilon_0(\varepsilon_1-i\varepsilon_2)]$.

In this paper, a novel and economical method for production of ferrite films was developed based on the sol-gel technique. The effects of annealing conditions of stoichiometric Ni–Zn ferrite sol-gel thin films on the physical and magnetic properties as well as on the dielectric losses in the frequency range 2–15 GHz have been investigated. The heating behavior of the Ni–Zn ferrite has been studied at 2.4 GHz, and the role of the grain size on microwave heating was examined.

II. EXPERIMENTAL PROCEDURE

A. Sol-gel synthesis of $Ni_{0.5}Zn_{0.5}Fe_2O_4$ films

Nickel zinc ferrites were prepared by the citrate precursor method.[28] Iron (III) nitrate nonahydrate, nickel nitrate hexahydrate, and zinc nitrate hexahydrate (all from Aldrich Co., ACS grade) were used as precursors for the preparation of the starting sol. The precursors were dissolved in ethanol in a molar ratio of Ni:Zn:Fe=1:1:4. Then the former salt solution was dissolved into the citric acid solution and stirred for 12 h. This solution was titrated quantitatively by an ammonia solution to a pH of 2. The resulting sol was dropped on a 1.0×1.0 cm^2 Si plate and spin-coated for 25 s at 3500 rpm with an acceleration rate of 1250 rpm/s. Drying was performed in an oven at 353 K for 30 min and then it was kept at temperatures 673, 873, 973, or 1073 K for 1 or 3 h, respectively. A part of the corresponding sols was dried in an oven at 353 K to get the powder.

B. Microstructure and magnetic properties characterization

Thermogravimetric analysis was carried out in an air flow (50 cm^3/min) with a heating rate of 10 K/min from room temperature to 973 K. The initial mass of the sample was 20 mg. X-ray diffraction (XRD) patterns were recorded at a scanning rate of 0.3° 2-theta/min using an x-ray diffractometer (Rigaku) with nickel filtered Cu K_α radiation produced at 40 kV and 27.5 mA. The microstructure analysis was performed with a scanning electron microscope (SEM, Quanta 3D FEG, FEI) operated at 20 kV and with atomic force microscopy (AFM, The NanosurfeasyScan 2) by using a contact mode.

X-ray photoelectron spectroscopy (XPS) measurements were carried out with a Kratos AXIS Ultra spectrometer, equipped with a monochromatic Al K_α x-ray source and a delay-line detector. Spectra were obtained using the aluminum anode (Al K_α=1486.6 eV) operating at 150 W. The background pressure was 2×10^{-9} mbar.

The hysteresis loop, remnant magnetization (M_r), saturation magnetization (M_s), and coercivity (H_c) of the composite films were measured at 295 and 355 K by means of a vibrating sample magnetometer equipped with a 2 T electromagnet and a furnace. M_s, M_r, H_c, and hysteretic losses were evaluated from hysteresis curves. The microwave absorption properties of the powders were determined at 2.4 GHz in a multimode microwave cavity at a constant power input of 100 W.

A near field evanescent microwave microscope was used to characterize the dielectric properties of the ferrites through frequency shift and quality factor measurements. The relative sensitivity of the microscope is in the range of 10^{-2} and the resolution is governed by the radius of the probe tip.[29] The microwave probe consists of a tuned $\lambda/4$ coaxial transmission line with an end wall aperture. A transverse electromagnetic wave created by a frequency generator moves along the coaxial probe and is totally internally reflected at the surface of the end wall aperture. The evanescent waves emanate from a sharpened tip extending concentrically through the aperture and interact with the sample. The coaxial microwave probe is capacitively coupled to the film, and to a Hewlett-Packard 8722ES network analyzer through a tuning network.

The resonant frequency and quality factor data are produced by setting the reference resonant frequency and the quality factor at approximately 10 μm above the sample sur-

face and moving the probe tip in micrometer steps to the position almost touching the surface of the film at 295, 315, 335, and 355 K. The resonant frequency and quality factor shift data is best fitted by a method of images model that produces the real and complex parts of the permittivity.[30]

Coplanar waveguide (CPW) test structures were used for experimental evaluation of the scattering parameter S_{21} of the ferrite films. The insertion loss of the circuit under measurement (S_{21}) represents the ratio of the output to the input power in decibel. The S_{21} is determined over the frequency range of 1–18 GHz based on appropriate impedance matching at both the source and load ends. The test structures were fabricated on bare substrates as well as on the thin film test samples for determination of attenuation and phase constants with and without the ferrite thin films.[31–33]

III. THEORY

The extraction of data through evanescent microwave microscopy requires detailed knowledge of the field configuration outside the probe-tip region.[34] The fundamental assumption of the theory is that the presence of the film introduces a perturbation to the existing electromagnetic field distribution. The changes in resonant frequency and reciprocal quality factor are described by Eqs. (1)–(3) (Ref. 35)

$$-2\frac{\Delta f}{f}-i\Delta\left(\frac{1}{Q}\right)=\frac{\int_V(\Delta\varepsilon\vec{E}_0^*\cdot\vec{E})dV}{\int_V(\varepsilon\vec{E}_0^*\cdot\vec{E})dV}, \tag{1}$$

$$\frac{\Delta f}{f}=\frac{(f-f_0)}{f}, \tag{2}$$

$$\Delta\left(\frac{1}{Q}\right)=\frac{1}{Q}-\frac{1}{Q_0}, \tag{3}$$

where $\vec{E}_0$ is the unperturbed electric field, $\vec{E}$ is the perturbed field, V is the volume of a region outside the resonator tip, f and Q are the perturbed resonant frequency and quality factor, and f_0 and Q_0 are the reference (or unperturbed) resonant frequency and quality factor, respectively.

The right hand side of Eq. (1) is a complex number dependent on the local complex permittivity, describing the dielectric properties of the films. Although this can be solved for the general case, let us restrict our discussion to the case when the tip touches the film (g is the distance between a tip and a film)

$$\frac{\Delta f}{f(g=0)}=\frac{f(g=0)-f_0}{f(g=0)}=\frac{1}{2}\mathrm{Re}\left[1+\frac{\ln(1-b)}{b}\right], \tag{4}$$

$$\Delta\left(\frac{1}{Q}\right)=\frac{1}{Q(g=0)}-\frac{1}{Q_0}=\mathrm{Im}\left[1+\frac{\ln(1-b)}{b}\right], \tag{5}$$

and

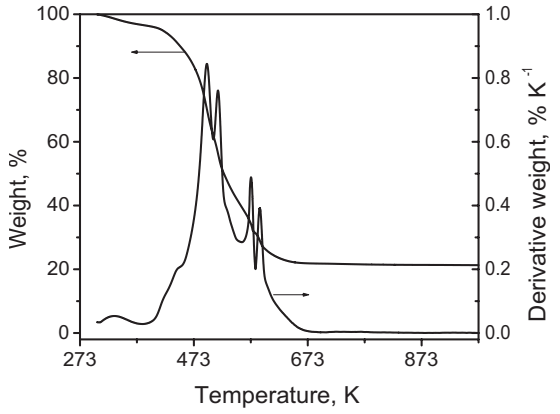

FIG. 1. The TG-DTG of $Ni_{0.5}Zn_{0.5}Fe_2O_4$ powder. Heating rate 10 K/min.

$$b=\frac{\varepsilon_1-1-i\varepsilon_2}{\varepsilon_1+1-i\varepsilon_2},\quad \varepsilon_2=\frac{\varepsilon''}{\varepsilon_0},\quad \varepsilon_1=\frac{\varepsilon'}{\varepsilon_0},\quad \varepsilon/\varepsilon_0=\varepsilon_1-i\varepsilon_2. \tag{6}$$

When the resonator tip approaches the surface of the film, the resonant frequency (f) and the quality factor (Q) will change. In measuring the frequency shift and the quality factor, the reference resonant frequency f_0 and corresponding Q_0 are set at a significant distance above the film (theoretically at infinity). This distance between the probe tip and the film should be sufficient to make sure that the evanescent field from the tip is not interacting with the film. Typical experimental data for the resonant frequency and quality factor were collected for a film-tip distance g=0 and 10 μm. The changes in resonant frequency and quality factor between these two extreme positions therefore amount to

$$\frac{2(\Delta f)}{A\cdot f(g=0)}=1+\frac{x\cdot\ln\sqrt{(1-x)^2+y^2}-y\cdot\arctan\frac{y}{(1-x)}}{(x^2+y^2)}, \tag{7}$$

$$\left(\frac{1}{B}\right)\Delta\left(\frac{1}{Q}\right)=\frac{x\cdot\arctan\frac{y}{(1-x)}+y\cdot\ln\sqrt{(1-x)^2+y^2}}{x^2+y^2}, \tag{8}$$

where

$$x=\frac{\alpha}{\beta},\quad y=\frac{2\varepsilon_2}{\beta},\quad \alpha=\varepsilon_1^2+\varepsilon_2^2-1,\quad \beta=(\varepsilon_1+1)^2+\varepsilon_2^2 \tag{9}$$

Substituting the values $A=7.044\times10^{-5}$ and $B=4.12\times10^{-5}$ determined experimentally, we can solve Eqs. (7) and (8) with respect to x and y. By using Eq. (9) we finally arrive at the effective values of the complex permittivity and the loss tangent ($\tan\delta=\varepsilon_2/\varepsilon_1=\varepsilon''/\varepsilon'$).

IV. RESULTS AND DISCUSSION

A. Thermal decomposition study

Figure 1 shows the thermogravimetry-differential ther-

TABLE I. Size and structure of calcined films.

Sample code	Calcination temperature (K)	Calcination time (h)	Crystal structure[a]	XRD average size[b] (nm)
A	673	1	S+H	<10
B	873	1	S	12
C	973	1	S	21
D	1073	1	S	24
E	1073	3	S	27

[a]S=spinel, H=hematite, α-Fe_2O_3.
[b]Calculated from the Scherrer formula using reflection planes (3 1 1).

mogravimetral (TG-DTG) (analysis) curves of the obtained powder at the temperature range of 300–973 K. It can be seen from Fig. 1 that the decomposition process of the powder consists of several stages. First, adsorbed water is removed from the $(N_2H_5)_3Ni_{0.5}Zn_{0.5}Fe_2(N_2H_3COO)_9 \cdot 3H_2O$ citrate precursor below 393 K. This corresponds to approximately 5.5% of the total weight loss which is in agreement with the theoretical value (5.4 wt %). The second stage at 433–513 K is related to a partial decomposition reaction of the citrate precursor.[36] This corresponds to 55% of the total weight loss. The minor weight loss in the range of 513–673 K (19 wt %) corresponds to the combustion of residual citric and a small quantity of carbon.[36] The overall weight loss is 78.8 wt % which is close to the theoretical value (76.3 wt %).

In order to get the films without microcracks, the calcination treatment was performed at a slow heating rate of 2 K/min below 673 K and at a higher rate of 5 K/min up to 1173 K.

B. Structural analysis

Five thin films calcined at different temperatures and time intervals were used in this study (Table I). Figure 2 shows the XRD patterns of the as-prepared samples A, B, D, and E. All the peaks could be assigned to a single spinel phase. An increase in grain size with increasing calcination temperature and time is clearly observed from the narrowing of the XRD lines. The average crystallite size has been calculated from the (311) diffraction peak using Scherrer's formula. The lattice constant of the NiZn ferrite films was 8.383 Å. This value is smaller than that of 8.410 Å previously reported for $Ni_{0.5}Zn_{0.5}Fe_2O_4$ nanopowders.[37]

The evolution of the microstructure of the sintered specimens with variations in the calcination temperature was observed in SEM and AFM micrographs. As can be seen from Fig. 3 the films calcined at 1073 K are homogeneous with very dense microstructures and they have high adhesion to the substrate. The film E demonstrates obvious grain growth and few pores. There were no microcracks in the films and film A was amorphous (not shown).

Film B revealed well-developed grains and fewer pores in comparison to the others with appreciable differences between them. The grains slowly appeared with increasing temperature and diameters of these grains are increasing also very slowly. A fine grain structure with grain sizes ranging from 20–50 nm is obtained.

Figure 4 shows AFM line profiles for samples B, D, and E. Sample C have a similar profile to that of sample D (not shown). The film thickness was estimated to be 1 μm. It can be seen that sample B has a low surface roughness with a difference between the highest and the lowest points of topography below 30 nm. Both samples D and E have much larger surface roughness with differences between peaks and troughs in the order of 140 nm.

Figure 5 presents the particle size distribution obtained from an AFM image of film E. The average size and the standard deviation obtained from the analysis of the histogram were 52.6 ± 6 nm. XRD data showed the presence of crystalline particles, with sizes of 26.9 nm. These results are of the same order of magnitude, although the AFM measurements systematically exhibit higher values. This tendency can be understood by considering the interaction between the specimen surface and the tip of the AFM probe. If the par-

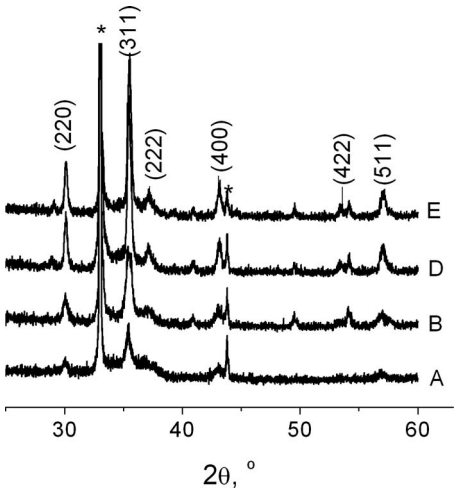

FIG. 2. XRD of films with a nominal composition of $Ni_{0.5}Zn_{0.5}Fe_2O_4$ calcined at different temperatures: (a) sample A 673 K for 1 h, (b) sample B 873 K for 1 h, (c) sample D 1073 K for 1 h, and (d) sample E 1073 K for 3 h. Reflections from the Si substrate are marked with an asterisk.

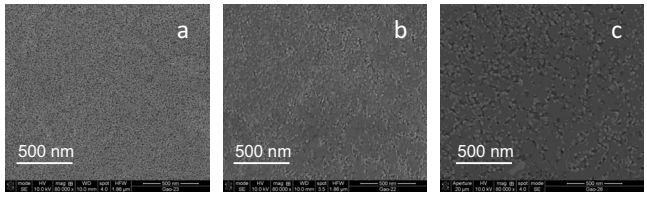

FIG. 3. SEM images of the NZF films calcined at different temperatures: (a) sample B, (b) sample D, and (c) sample E.

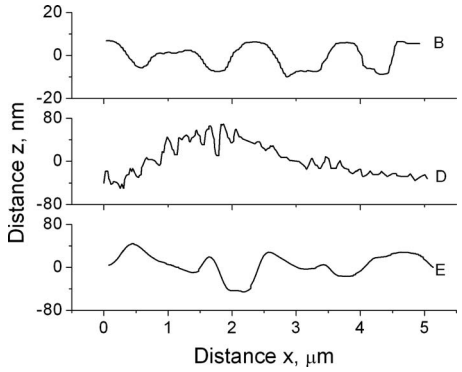

FIG. 4. AFM scans along the surface of the NZF films B, D, and E.

ticles are dispersed on the substrate surface, the lateral interaction between the tip and the particles leads to a distortion of their shape and to an overestimation of the measured dimensions.[38,39]

C. EDS/XPS analysis

The presence of Zn, Ni, and Fe in the films was revealed by energy dispersive spectroscopy analysis. The Ni:Zn:Fe ratio was close to the stoichiometric one for Ni and Fe within the error of the EDS system, while the data suggest a slight deficiency of Zn by a few atomic percents in the films as compared with that in the initial solutions (see Table II). The Fe, Ni, and Zn concentrations in the films remained constant irrespective of the position and calcination conditions.

The chemical composition and the purity of the samples were checked by XPS analysis. The relative elemental concentrations were used to estimate the atomic composition of the deposited films, by considering their values normalized to the nominal composition (see Table II).

A surface composition analyzed by XPS showed the Fe:Zn:Ni ratio of 4.5:0.5:0.5 indicating that the film surface was enriched in iron. The surface enrichment in iron occurred due to different mobility of the cations in the oxygen lattice during the formation and growth of spinel grains. The binding energies of Fe, Ni, and Zn are depicted in Fig. 6. The binding energy of Fe $2p_{3/2}$ was in the range from 711.3 to 710.5 eV. The presence of Fe^{3+} was confirmed by a satellite peak at around 8.0 eV above the principal peak.[40,41] An increase in the calcination temperature to 1073 K does not significantly change the Fe $2p_{3/2}$ binding energy which is in agreement with literature data.[41] The binding energy of Ni^{2+} of 855.1 eV (sample A) reduced slightly toward 854.9 eV at the highest calcination temperature (sample E) (Fig. 6). The peak shape of Ni $2p_{3/2}$ in NiO and spinel is different.[41] There is a shoulder (satellite peak) in NiO while no such shoulder is reported in the spinel structure. Therefore it can be concluded that samples B–E contain all Ni in the spinel structure. The binding energy of Zn^{2+} monotonously decreased with the increasing temperature confirming transformation of the mixed oxide to a ferrite spinel structure.[42]

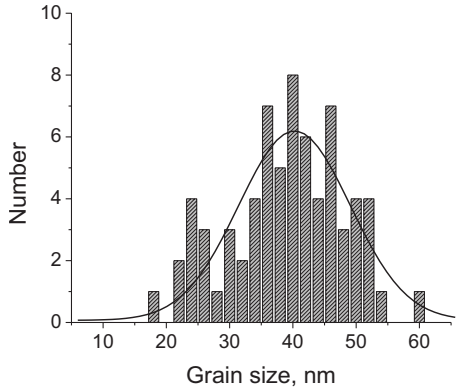

FIG. 5. Particle size distribution, determined from AFM images, for the NiZn ferrite film (sample E).

TABLE II. Elemental analysis of film D from the EDS data.

Sample code	wt %	at. %	Relative atomicratio
Fe	4.58	2.22	2.0
Ni	1.15	0.53	0.48
Zn	1.08	0.45	0.41

D. Magnetic properties

The average crystallite sizes, calculated using the Scherrer equation from the XRD peaks, were found to vary from less than 10 to 26.9 nm for the samples under investigation (Table I). The characteristics of the hysteresis loop, the coercivity, and the saturation magnetization, are shown in Fig. 7(a) while the remnant magnetization and hysteresis loss are presented in Fig. 7(b) as a function of the average crystallite size at 295 and 355 K.

It is can be seen from Fig. 7(a) that the saturation magnetization monotonously increases with increasing the calcination temperature from 873 to 1073 K and duration of calcination from 1 to 3 h at 1073 K. However, the highest value of 47.5 J/T/kg obtained for the largest grain size remains lower than that of the bulk ferrite particles (60 J/T/kg).[43] The magnetizing mechanism of soft ferrites results from spin domain rotation and domain walls motion. In turn, domain walls motion is affected by the grain size and the sintering density,[44,45] and is enhanced by the increase in the grain size.[46,47] In smaller grains, an increased surface to volume

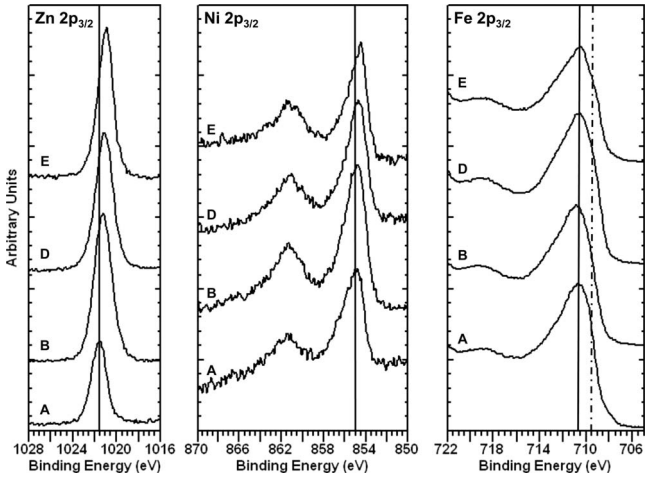

FIG. 6. XPS spectra for Zn, Ni, and Fe in samples A, B, D, and E.

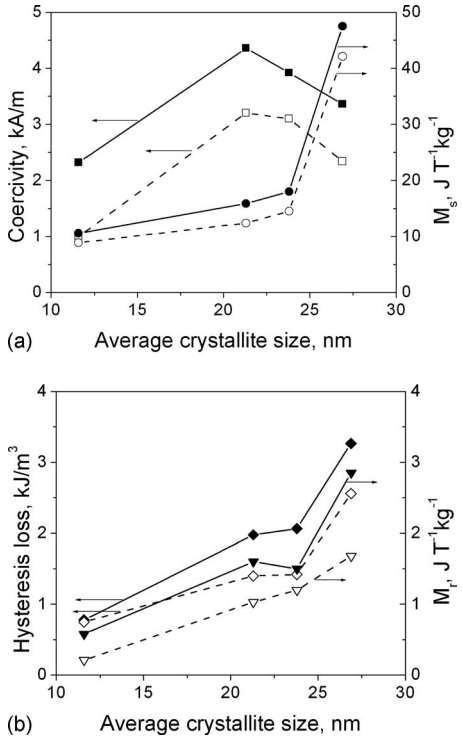

FIG. 7. (a) Coercivity and saturation magnetization (M_s); (b) hysteresis loss and remnant magnetization (M_r) as a function of crystallite size. Solid lines and closed symbols: measurements at 295 K, dashed lines and open symbols: measurements at 355 K.

ratio leads to a noncollinearity of magnetic moments on the surface.[48,49] This causes a decrease in the saturation magnetization with a decrease in the grain dimensions.

The change in the average crystallite size influenced the coercivity of the ferrite samples as it is also shown in Fig. 7(a). The coercivity increases with increasing diameter until it reaches a maximum value at the critical diameter. A further drop of H_c for the films calcined at 1073 K originates from the transition of the magnetic single domain to the magnetic multidomain within a single grain. The critical diameter (d_{cr}) can be calculated using Eq. (10) (Ref. 50)

$$d_{cr} = \frac{9 \times 10^{-7} \varepsilon_p}{2\pi M_s^2}, \tag{10}$$

where ε_p as the surface energy of the domain wall is defined as follows:

$$\varepsilon_p = \left(\frac{2 k_B T_C K_1}{a} \right)^{0.5}, \tag{11}$$

where k_B is the Boltzmann constant (1.38×10^{-23} J/K), T_c is the Curie temperature [T_c=425 K (Ref. 51)], K_1 is the magnetocrystalline anisotropy constant [1.5×10^3 J/m^3 (Ref. 52)], a is the lattice parameter (8.41×10^{-10} m), and M_s is the spontaneous magnetization [3.1×10^{-2} T (Ref. 43)]. The critical diameter calculated by Eq. (10) is 21.6 nm. This value is in good agreement with the experimental value of 21 nm.

The maximum value of the coercivity was 4.4 kA/m (54 Oe) for the grain size of 21 nm. This H_c value is larger than that of 41 Oe reported by Caizer and Stefanescu[52] for 29 nm

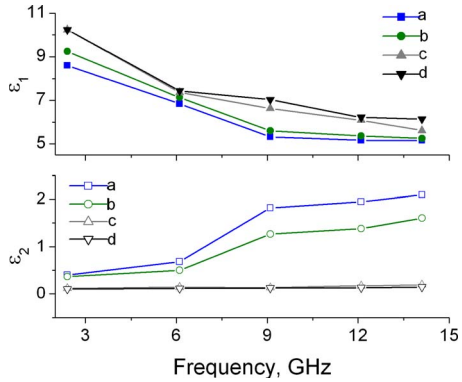

FIG. 8. (Color online) Real (ε_1) and imaginary (ε_2) parts of the relative complex permittivity measured for sample E at different temperatures: (a) 295 K, (b) 315 K, (c) 335 K, and (d) 355 K.

$Ni_{0.35}Zn_{0.65}Fe_2O_4$ nanoparticles, while it is smaller than that of 90 Oe reported by Albuquerque *et al.*[53] for $Ni_{0.5}Zn_{0.5}Fe_2O_4$ nanoparticles with a mean size of 39 nm. In the latter study, the authors concluded that Ni atoms occupy octahedral B sites only, whereas Zn atoms occupy tetrahedral A sites in accordance with the minimum lattice energy in the spinel structure. In the single domain region, the coercivity decreases when the particle size is reduced, since the alignment of the magnetic moments inside the domain is fully controlled by thermal energy, resulting in superparamagnetic behavior. Film B showed superparamagnetic behavior as can be concluded from almost closed M-H loops with a hysteresis loss below 0.8 kJ/m^3 [Fig. 7(b)].

The remnant magnetization increases from 0.6 to 2.9 J/T/kg with increasing the grain size from 11 to 26.9 nm [Fig. 7(b)]. The latter value coincides with that reported for $Ni_{0.5}Zn_{0.5}Fe_2O_4$ ferrite nanoparticles with a size of 20 nm.[54] The increase in remnant magnetization is also attributed to an increase in the mean grain size. The magnetic parameters obtained at 355 K temperature show the same tendency as those measured at 295 K.

E. Microwave losses

The real and imaginary parts of the relative permittivity (ε_1 and ε_2, respectively) as a function of frequency in the range from 2 to 15 GHz were calculated from Eqs. (7) and (8). Figures 8 and 9 show the dependence of the permittivity

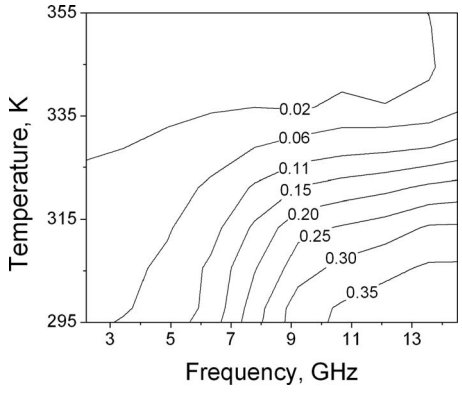

FIG. 9. Loss tangent as a function of temperature and frequency for sample E.

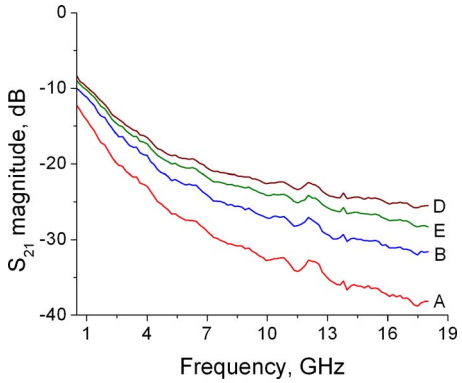

FIG. 10. (Color online) Reflection loss at 295 K as a function of frequency for samples A, B, D, and E.

on the frequency for ferrite film E at 295, 315, 335, and 355 K and its loss tangent as a function of frequency and temperature. It is clearly seen from these figures that the losses are the largest for high frequencies and low temperatures (Fig. 9) due to roughly a linear decrease in ε_1 (from ~8 to ~5) with frequency independently of the temperature. These values are close to those of 6.5–5.5 reported for $Ni_{0.5}Zn_{0.5}Fe_2O_4$ ferrite materials in the 1–15 GHz range[55,56] at room temperature. The real part of the permittivity slightly increased with an increase in temperature from 295 to 355 K. In the same range of frequencies, the imaginary part of the permittivity (ε_2) increases, contributing to the overall increase in the loss tangent with frequency. These data are also in a good agreement with those reported in Ref. 56, where ε_2 values were around 0.5 and slightly increased at higher frequencies.

The insertion loss of the circuit under measurement (S_{21}) is a complex quantity with a magnitude and phase. The magnitude of S_{21} determines the loss within the CPW transmission line and is used to estimate the attenuation constant, while the phase represents the electrical length of the line and is used to estimate the phase constant. The magnitude of S_{21} itself represents transmission and is plotted in Fig. 10 as a function of frequency between 1 and 18 GHz. Transmission losses were as low as −35 dB for film A. The largest loss is observed again for ferrite film D at the highest frequency.

The heating curves in Fig. 11 show that the grain size strongly affects the heating process. In addition to the study of the heating behavior of the ferrite films, the effect of the Si substrate was also studied. The volume and heat capacity of the Si substrate are larger than these of ferrite films. Therefore, the substrate absorbs most of the thermal energy that is converted from microwave energy. It can be seen from Fig. 11, that the trend in the heating curves follows the trend in the film transmission curves in Fig. 10. The highest heating rate at 2.4 GHz was observed for the sample with the grain size close to the critical size calculated by Eq. (10). The temperature change in microwave heating reaches a steady-state value when the flux of the thermal energy generated from the microwave absorption becomes equal to the thermal energy loss to the environment (Fig. 11). It appears that deposition of film A with a mixed ferrite+hematite structure increases the reflection losses of the substrate which decreases the heating rate as compared with pure ferrite films.

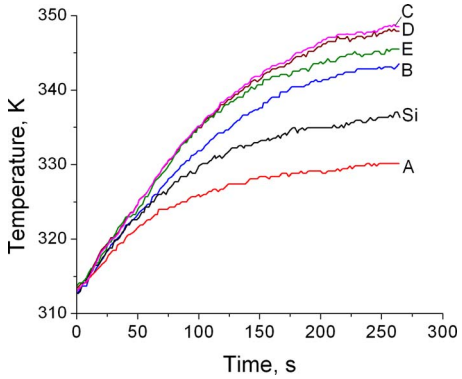

FIG. 11. (Color online) Heating curves at 2.4 GHz for samples A–E and a Si substrate plate used as a reference material.

V. CONCLUSIONS

A hydrothermal process was employed to produce single-phase, highly crystalline, nanometric $Ni_{0.5}Zn_{0.5}Fe_2O_4$ mixed ferrite films with a thickness of 1 μm. The average size of the nanocrystallites ranging from 12–27 nm can efficiently be controlled by modifying the calcination temperature between 873 and 1073 K and the calcination time between 1 and 3 h. The saturation and remnant magnetization increased with increasing the grain size, while the coercivity demonstrated a maximum near a critical grain size of 21 nm due to the transition from monodomain to multidomain behavior. This value was in a good agreement with that resulted from the calculation taking into account the surface effects, particle shape, and interactions. The highest heating rate in a multimode cavity at 2.4 GHz was observed for the ferrite films subjected to calcination at 973 and 1073 K for 1 h. This conclusion is based on experimental results from evanescent microwave microscopy and direct microwave heating measurements. A feasible way to prepare NiZn ferrite films as a microwave absorber by controlling the grain size by calcination temperature and calcination time has been demonstrated. The Ni–Zn ferrite thin films can be prepared on the walls of microstructured reactors for efficient and fast microwave heating allowing nonsteady-state operation.

[1]C. S. Kim, Y. S. Yi, K.-T. Park, H. Namgung, and J.-G. Lee, J. Appl. Phys. **85**, 5223 (1999).
[2]A. K. Srivastava, M. J. Hurben, M. A. Wittenauer, P. Kabos, C. E. Patton, R. Rameh, P. C. Dorsey, and D. B. Chrisey, J. Appl. Phys. **85**, 7838 (1999).
[3]M. M. Amado, M. S. Rogalski, L. Guimarães, J. B. Sousa, I. Bibicu, R. G. Welch, and S. B. Palmer, J. Appl. Phys. **83**, 6852 (1998).
[4]C. N. Chinnasamy, A. Narayanasamy, N. Ponpandian, K. Chattopadhyay, K. Shinoda, B. Jeyadevan, K. Tohji, K. Nakatsuka, T. Furubyashi, and I. Nakatani, Phys. Rev. B **63**, 184108 (2001).
[5]X. Li and Q. Li, J. Alloys Compd. **458**, 558 (2008).
[6]J. Pattanayak, J. Mater. Sci. Lett. **10**, 1461 (1991).
[7]A. Dias, R. L. Moreira, and N. D. S. Mohallem, J. Phys. Chem. Solids **58**, 543 (1997).
[8]A. Dias, N. D. S. Mohallem, and R. L. Moreira, Mater. Res. Bull. **33**, 475 (1998).
[9]K. Iwauchi, Jpn. J. Appl. Phys., Part 1 **10**, 1520 (1971).
[10]T. Sato, K. Haneda, M. Seki, and T. Iijima, Appl. Phys. A: Solids Surf. **50**,

13 (1990).
[11]C. N. Chinnasamy, A. Narayanasamy, N. Ponpandian, K. Chattopadhyay, H. Gueralt, and J.-M. Greneche, J. Phys.: Condens. Matter **12**, 7795 (2000).
[12]H. H. Hamdeh, J. C. Ho, S. A. Oliver, R. J. Willey, G. Oliveri, and G. Busca, J. Appl. Phys. **81**, 1851 (1997).
[13]A. H. Morr and K. Haneda, J. Appl. Phys. **52**, 2496 (1981).
[14]A. T. A. Wee, J. P. Wang, A. C. H. Huan, L. P. Tan, R. Gopalakrishnan, and K. L. Tan, IEEE Trans. Magn. **33**, 2986 (1997).
[15]A. Lisfi, J. C. Lodder, P. de Haan, M. A. Smithers, and F. J. G. Roesthuis, IEEE Trans. Magn. **34**, 1654 (1998).
[16]A. Takayama, M. Okuya, and S. Kaneko, Solid State Ionics **172**, 257 (2004).
[17]A. Verma, T. C. Geol, and R. G. Mendiratta, J. Magn. Magn. Mater. **208**, 13 (2000).
[18]T. Sugimoto, Y. Shimotsuma, and H. Itoh, Powder Technol. **96**, 85 (1998).
[19]R. Hochschild and H. Fuess, J. Mater. Chem. **10**, 539 (2000).
[20]A. Dias and R. L. Moreira, Mater. Lett. **39**, 69 (1999).
[21]M. Sedlár, V. Matejec, T. Grygar, and J. Kadlecová, Ceram. Int. **26**, 507 (2000).
[22]W. Liu and J. Wu, Mater. Chem. Phys. **69**, 148 (2001).
[23]N. D. S. Mohallem and L. M. Seara, Appl. Surf. Sci. **214**, 143 (2003).
[24]W. Yan, L. Wang, Z. Xia, M. Cheng, Q. Li, and Y. Zhang, Mater. Res. Bull. **42**, 1468 (2007).
[25]R. A. Kleismit, M. ElAshry, G. Kozlowski, M. S. Amer, M. K. Kazimierczuk, and R. R. Biggers, Supercond. Sci. Technol. **18**, 1197 (2005).
[26]X. D. Xiang and C. Gao, Mater. Charact. **48**, 117 (2002).
[27]R. A. Kleismit, K. Munbodh, J. J. Boeckl, A. L. Campbell, K. K. Koziol, G. Kozlowski, S. C. Hopkins, and T. L. Peterson, J. Nanosci. Nanotechnol. **9**, 4543 (2009).
[28]E. E. Sileo, R. Rotelo, and S. E. Jaboco, Physica B **320**, 257 (2002).
[29]R. A. Kleismit, G. Kozlowski, and M. K. Kazimierczuk, IEEE Trans. Appl. Supercond. **54**, 639 (2006).
[30]R. A. Kleismit, G. Kozlowski, R. R. Biggers, I. Maartense, M. K. Kazimierczuk, and D. B. Mast, IEEE Trans. Microwave Theory Tech. **54**, 639 (2006).
[31]J. C. Booth, L. R. Vale, and R. H. Ono, *Tunable RF and Microwave Devices*, MRS Symposia Proceedings Vol. 603 (Materials Research Society, Pittsburgh, 2000), p. 253.
[32]M. D. Janezic, D. F. Williams, V. Blaschke, A. Karamcheti, and C. S. Chang, IEEE Trans. Microwave Theory Tech. **51**, 132 (2003).
[33]G. Subramanyam, P. Mathala, and S. Kanagala, Invited Talk, Asia Pacific Microwave Conference, New Delhi, 2004 (unpublished).
[34]R. A. Kleismit, A. L. Campbell, G. Kozlowski, T. J. Haugan, R. R. Biggers, I. Maartense, S. C. Hopkins, P. L. Barnes, and T. L. Peterson, Supercond. Sci. Technol. **21**, 035008 (2008).
[35]G. Kozlowski, R. Kleismit, J. Boeckl, A. Campbell, K. Munbodh, S. Hopkins, K. Koziol, and T. Peterson, Physica E (Amsterdam) **41**, 1539 (2009).
[36]X. Feng, Z. Xiangchun, L. Liangchao, L. Hui, and J. Jing, J. Rare Earths **25**, 232 (2007).
[37]P. Ravindranathan and K. C. Patil, J. Mater. Sci. **223**, 261 (1987).
[38]A. Dias, V. T. L. Buono, J. M. Vilela, M. S. Andrade, and T. M. Lima, J. Mater. Sci. **32**, 4715 (1997).
[39]A. Dias, R. L. Moreira, N. D. S. Mohallem, J. M. C. Vilela, and M. S. Andrade, J. Mater. Res. **13**, 223 (1998).
[40]J.-P. Jolivet, C. Chanéac, and E. Tronc, Chem. Commun. (Cambridge) **2004**, 481.
[41]V. K. Mittal, S. Bera, R. Nithya, M. P. Srinivasan, S. Vermurugan, and S. V. Narasimhan, J. Nucl. Mater. **335**, 302 (2004).
[42]L. S. Dake, D. R. Baer, and J. M. Zachara, Surf. Interface Anal. **14**, 71 (1989).
[43]J. Smit and H. P. J. Wijn, *Ferrites* (Philips Technical Library, Eindhoven, The Netherlands, 1959), p. 157.
[44]R. H. Kodama, A. E. Berkowitz, E. J. McNiff, and S. Foner, Phys. Rev. Lett. **77**, 394 (1996).
[45]C. Caizer, J. Magn. Magn. Mater. **251**, 304 (2002).
[46]H. Zhang, Z. Ma, J. Zhou, Z. Yue, L. Li, and Z. Gui, J. Magn. Magn. Mater. **213**, 304 (2000).
[47]M. P. Bogdanovich, Sov. Phys. Solid State **33**, 1952 (1991).
[48]C. Caizer, Mater. Sci. Eng., B **100**, 63 (2003).
[49]K. Haneda and A. H. Morrish, J. Appl. Phys. **63**, 4258 (1988).
[50]I. Z. Rahman and T. T. Ahmed, J. Magn. Magn. Mater. **290–291**, 1576 (2005).
[51]H. N. W. Lekkerkerker and W. G. Laidlaw, J. Phys. (Paris) **38**, 1 (1977).
[52]C. Caizer and M. Stefanescu, Physica B **327**, 129 (2003).
[53]A. S. Albuquerque, J. D. Ardisson, W. A. A. Macedo, and M. C. M. Alves, J. Appl. Phys. **87**, 4352 (2000).
[54]K. H. Wu, Y. C. Chang, T. C. Chang, Y. S. Chiu, and T. R. Wu, J. Magn. Magn. Mater. **283**, 380 (2004).
[55]Y. Hwang, Mater. Lett. **60**, 3277 (2006).
[56]C.-H. Peng, H.-W. Wang, S.-W. Kan, M.-Z. Shen, Y.-M. Wei, and S.-Y. Chen, J. Magn. Magn. Mater. **284**, 113 (2004).